Building and Characterization of Laser diodes as well as System design of a Dual Wavelength Fabry-Perot Interferometer

A Senior Project
presented to
the Faculty of the Physics Department
California Polytechnic State University, San Luis Obispo

In Partial Fulfillment
of the Requirements for the Degree
Bachelor of Science

by
Nicholas Czapla
May, 2012

I. Introduction

The refractive index, *n*, of a material is a ratio of the speed of light in a vacuum to the speed of light in that material. The bigger the ratio, the bigger *n* becomes which indicates that light moves more slowly through the material. The refractive index has many uses; it is used to determine to focusing power of a lens, dispersive power of a prism, and can even be used to differentiate between two different materials. It is used often in chemistry to determine the content of aqueous solutions like DNA [aqueous solution][1]. It is important to know the refractive index accurately because fiber optics and radio communications rely heavily on the accuracy of the refractive indices and are so prevalent in today's society.

However, this is not always so easy; there are many complications that come with determining the refractive index of a given material. The biggest problem is that the refractive index is not constant for a given material; there are many things on which it depends. The two most common things are temperature and wavelength. The refractive index actually changes depending on the temperature of the material, or variation within the material. The best example of this is looking over asphalt on a hot day; the light from the "shiny" parts in the asphalt is actually light coming from the sky just above the horizon. As it approaches the hot pavement, it passes through hotter and hotter air and the light bends back up towards your eyes. The refractive index also depends on the wavelength of the light passing through it. The best example of this is passing white light through a prism; before the light goes through the prism it is only seen as one beam of white light, whereas after the light passes through the prism it is separated into its wavelengths, with each wavelength exiting at a different angle. You can see examples of the refractive index depending on the wavelength and temperature of the medium in figures 1a and 1b.

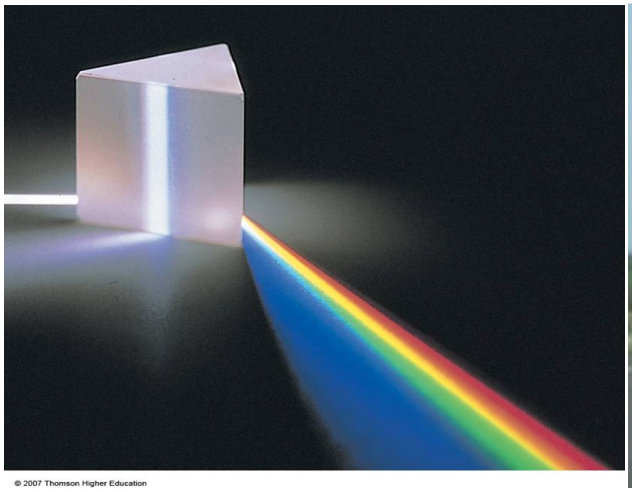

Figure 1a: Wavelength dependence of n.[2]

Figure 1b: Temperature Dependence of n.[3]

The goal of this projects a proof of theory to measure the refractive index of wafer shaped material using a two wavelength Fabry-Perot interferometer setup. Additionally, the thickness of the sample can also be determined without having to know any previous parameters of the material. The bulk of this work presents progress towards this goal including: building, testing and characterizing eight different laser diodes (two 639nm, two 850 nm, two 980 nm and two 1310nm) and designing and building a working experimental setup.

II. Previous methods for measuring *n*

All methods for measuring the refractive index of a material exploit the fact that light changes speed at the boundary between different media, and for angles other than normal incidence the light propagation direction will change. The change in direction of the light propagation can be determined using Snell's law,

$$n_1 \sin\theta_1 = n_2 \sin\theta_2 \tag{1}$$

where n_1 is the refractive index of the initial medium that the beam travels through, θ_1 is the angle of incidence on the prism, n_2 is the refractive index of the prism and $\theta_2$is the angle from normal in the new medium.

One of the oldest, and most accurate, ways of measuring the refractive index is the prism method, otherwise known as the minimum deviation angle. The theory behind it is that you can send light into a prism, with a known angle of the prism apex, at a known angle of incidence. By measuring the minimum angle of deviation from the lights prism-free path and using the equation below the refractive index of the prism can be determined,

$$n = \frac{\sin\left((\phi+\theta)/2\right)}{\sin(\phi/2)} \tag{2}$$

where n is the refractive index of the prism, θ is the angle of minimum deviation, ϕ is the relevant angle of the prism.[4]

However, there are a few limitations to the prism method. If the material you're trying to measure isn't a prism shape and you aren't able to carve it into one then the prism method won't work because it relies on knowing the angle of the corner of the prism you're using. It also makes the assumption that the refractive index is constant throughout the whole sample; however this is not always the case.

Most infrared optical materials are semiconductors. Semiconductors aren't produced as one solid uniform material; they're grown from a Silicon "seed". This is a fairly complex process that involves melting the Silicon into a seed in a vacuum chamber. You then "grow" the semiconductor in layers by pumping in gas of different elements or molecules that attached themselves to the seed. During the growing process, for binary and ternary semiconductors you

can change what you are pumping into the seed thereby changing the mixture of the growth at that particular height from the seed.[5] This position-dependent difference in the mixture of the semiconductor will definitely have an effect on the refractive index of the wafer at different heights.

The growth is cut into a wafer shape, a thin and flat object.[5,6] This is the perfect example of a sample that couldn't be cut into a prism shape because cutting any portion of the wafer into a prism shape would destroy its usefulness and, as mentioned before, you can't cut one wafer to know the refractive index of the rest of the batch because it can change with respect to the height from the seed.

An established, non-destructive method for measuring the refractive index of wafer shaped materials is using the Michelson Interferometer.[7,8,9] The Michelson Interferometer is an extremely accurate way to measure any path length difference, or change in path length of monochromatic light sources, light with a single wavelength. The setup involves a beam splitter, a reference path, a sample path, and another pellicle to combine the beams again (can be the original beam splitter). The interferometer first splits a monochromatic light source at the beam splitter. One half goes down the "reference path" that contains no sample or moving mirror. The second half goes down the "sample path" which contains either a moving mirror or, in this case, a rotating sample in the beam path which changes the sample path length as it rotates. The interferometer then combines the two beams again where they exit and propagate towards the detector. The setup can be seen in figure 2 below.

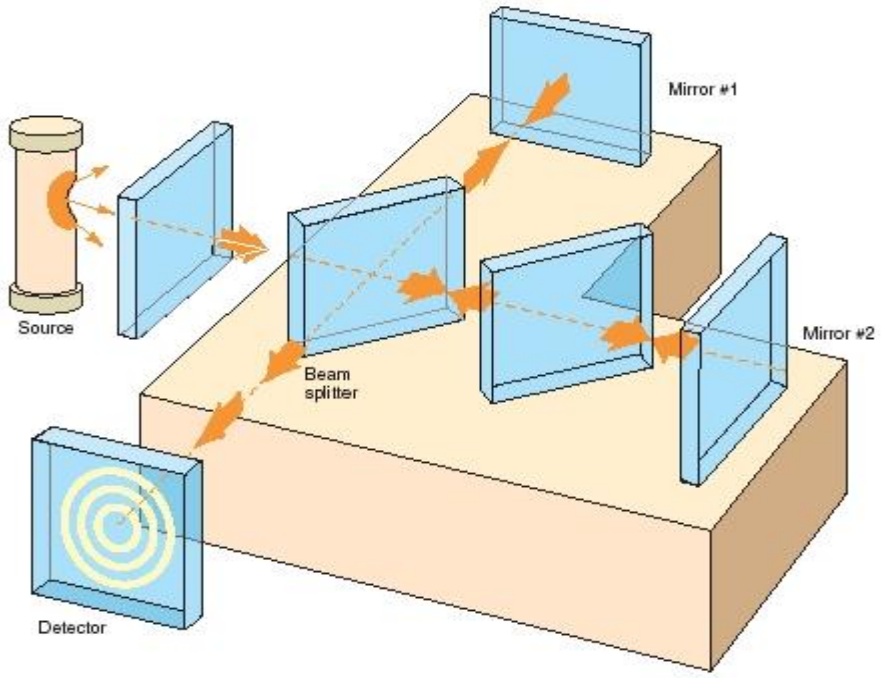

Figure 2: Michelson Interferometer setup.[10]

When the two beams are brought back together a difference in phases causes the two beams to constructively and destructively interfere creating a fringe pattern. Constructive interference is seen as the presence of bright light in the fringe pattern, in this paper they will be referred to as the "peaks" of the fringe pattern. Likewise, destructive interference is seen as an absence of light or dark lines in the fringe pattern. This fringe pattern typically presents itself as a bulls-eye pattern, and example of the bulls-eye pattern is shown below in figure 3.

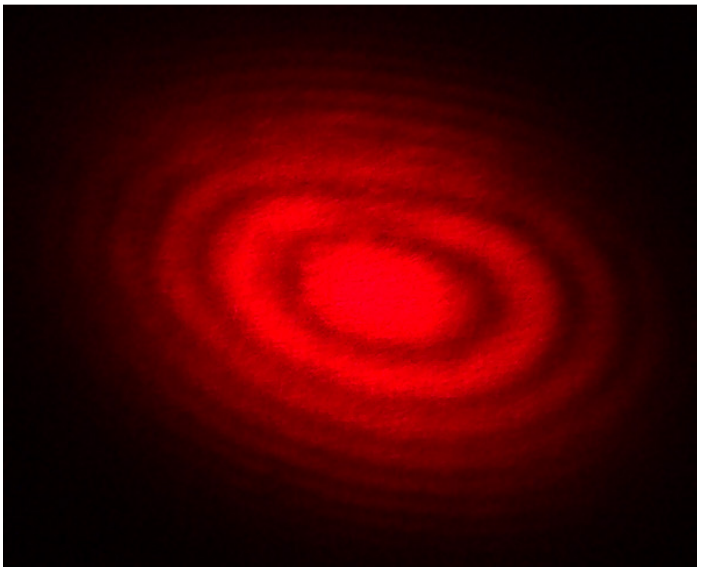

Figure 3: Michelson Interferometer Bulls-Eye.[11]

As the wafer sample rotates, the path length of the sample beam changes, changing the phase of the sample beam. This change in phase changes the type of interference at every position in the combined beam. The change in interference can be seen as the fringes moving, either to the left, right, up or down depending on how the sample is being rotated.[12] You can determine the location of the fringes by using

$$I_D = I_R^2 + I_S^2 + 2I_R I_S \cos\left[\frac{4\pi d}{\lambda}\left(\sqrt{n^2 - \sin^2\theta} + 1 - \cos\theta\right) + \phi_0\right] , \qquad (3)$$

where I_D is the intensity of the combined beam at the detector, I_R and I_S are the intensities of the reference and sample beam, respectively, λ is the wavelength of the beam, d is the thickness of the sample and θ is the angle of incidence of the beam on the sample. Places of pure constructive interference and destructive interference are found when the bigger cosine term is equal to integer multiples of π. The locations of these maximums and minimums can be fit to

$$m\pi = \frac{4\pi d}{\lambda}\left(\sqrt{n^2 - \sin^2(\theta - \theta_0)} - \cos(\theta - \theta_0) + 1\right) + \phi_0 \quad , \qquad (4)$$

where m is an integer, θ_0 and $\phi_0$are constants found from the data. θ_0 relates to any difference between the origin of the rotation stage and normal incidence of the laser path. The phase

constant, ϕ_0, accounts for any fringes due to the difference in optical path length at normal incidence. Using the angle of peaks you can determine the refractive index of the sample for a particular wavelength.[9]

The Michelson interferometer is a great non-destructive method for flat-parallel wafer samples. It is a good way to make sample specific measurements and to test the purity of sample.[10] You can see from equation 1 that *n* and *d* are multiplied by each other, meaning that they are not separable. Because of this, the experimental accuracy of one depends on the assumed, or known, accuracy of the other. This dependence on the accuracy of the material's width is the biggest limitation of this method. However, it's not the only problem with the Michelson; because the interferometer is so good at measuring minute differences in path length, typically on the nanometer scale, any changes to the setup can affect the results. Many things can affect the setup enough to be seen in the results; the vibrations from a car passing by or bumping the table will send ripples through the table and mirrors changing the path length, even changes in the air flow in the room can change the path length and subsequently, the results.

Another non-destructive method for determining the refractive index of wafer shaped material is using both a Michelson Interferometer and a Fabry-Perot Interferometer.[13] The brilliance of this method is in using the two different types of interferometers, Michelson and Fabry-Perot. This combination of the two allows you to accurately measure the thickness, *d*, and refractive index, *n*, without having to initially know either one very well. Unlike the method of just using the Michelson which produces an equation where *n* and *d* are not separable, this method combines the separate measured information about the phases from each interferometer and produces an equation where *n* and *d* have become decoupled. The Michelson interferometer works the same as before, only the Fabry-Perot needs explaining.

The Fabry-Perot interferometer still relies on the basic idea that a difference in phase causes constructive and destructive interference. However, the setup is much easier than the Michelson setup. It only involves a single monochromatic beam path going through a rotating sample. Instead of the phase difference coming from half of the beam going through a sample and combing with the reference beam, the phase difference comes from internal reflections of the beam inside the sample. Whenever a light source hits a change in medium there is a portion of the light that is reflected back into the original medium. This phenomenon happens again inside the sample and is shown in figure 4 below.

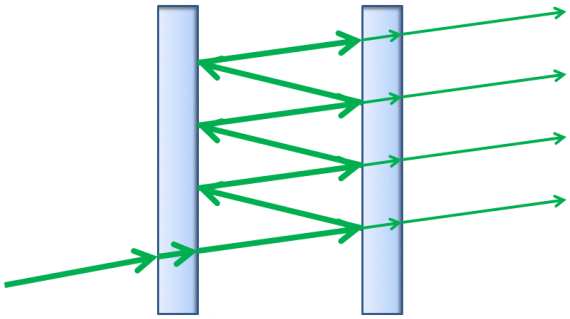

Figure 4: Internal Reflections inside a sample.[14]

Since only a portion of the light is being reflected at each media boundary there must be a portion that is transmitted. If the sample is flat then the transmitted light will be in the same direction. However, they can contain different phases from the difference in path lengths in the sample and the extra reflections off the boundary of the media. Unlike in the depiction of figure 4, in reality, the lateral displacement of each transmitted beam is very small with respect to the beams width. For thin (a few mm) samples only a "single" beam is observed to exit the sample. As with the Michelson this phase difference can be seen as a fringe pattern within the transmitted beam. As the sample is rotated, the path length inside the sample changes causing the phases to change which in turn causes a movement in the fringe pattern.[13,15] As stated earlier, the huge benefit of using this method is the fact that *n* and *d* can now be separated using the data collected from both the Michelson and the Fabry-Perot. The separation comes from the fact that both interferometers have different equations for the intensity of the fringes at the detector. The intensity of the light from the Fabry-Perot set is

$$I_D = \left[\frac{(1-r^2)^2}{1+r^4-2r\cos\phi_f}\right] I_0 \quad , \tag{5}$$

where I_D is the intensity of the beam at the detector, I_0 is the initial intensity of the beam, r is the reflection coefficient of the sample and ϕ_f is the angle dependent phase difference given by

$$\phi_f = \frac{4\pi d}{\lambda}\sqrt{n^2 - \sin^2\theta} \quad , \tag{6}$$

where d is the thickness of the sample, λ is the wavelength of the beam, n is the refractive index of the material and θ is the angle of incidence of the beam on the sample. Subtracting equation 4 from equation 2 produces the result that only depends on the thickness, *d*

$$\phi_m - \phi_f = \frac{4\pi d}{\lambda}(1 - \cos\theta) \quad . \tag{7}$$

This simple equation allows you to do what cannot be done with only the Michelson, accurately solve for both *d* and *n*. You can also fit the maximums and minimums of the Fabry-Perot fringes can be fit to

$$m\pi = \frac{4\pi d}{\lambda}\sqrt{n^2 - \sin^2(\theta - \theta_0)} + \phi_0 \quad . \tag{8}$$

After determining d from equation 5, n can be determined from either the Michelson or Fabry-Perot fringe data using either equation 2 or 6, respectively.

The huge benefit to this method is the fact that you can independently measure both *n* and *d* accurately. As with the just the Michelson interferometer, this combination is a great non-destructive way to measure wafer shaped material. The biggest problem with this method is the fact that this setup inherently has the problems of both interferometer setups. As before, with just the Michelson, this set up is extremely sensitive to outside interference, such as vibrations and air currents. The other complication that arises from the Fabry-Perot interferometer is the fact that the sample needs to have to extremely flat, parallel sides. This is because any curvature to either side of the sample will cause internal reflections to be "knocked" off course and not interfere with the original beam. The more internal reflections there are the more noticeable any curvatures to the sample become. An extreme example of non-parallel sides is a prism; as the prism rotates in the path of the beam the final beam is shifted accordingly.

III. Alternative Method for measuring *n*

Another, recently proposed, method for measuring the refractive index using interferometers uses a Fabry-Perot interferometer fringe pattern from two different monochromatic light sources to measure *n* and *d*. The method requires that two lasers are incident upon a sample at the same time and in the same spot. This method shows promise in terms of simplicity, speed and the ability to make refractive index measurements at two different wavelengths simultaneously.[16] This senior project is an exploration towards building and testing an experiment utilizing the method. This setup can be seen in figure 5, below.

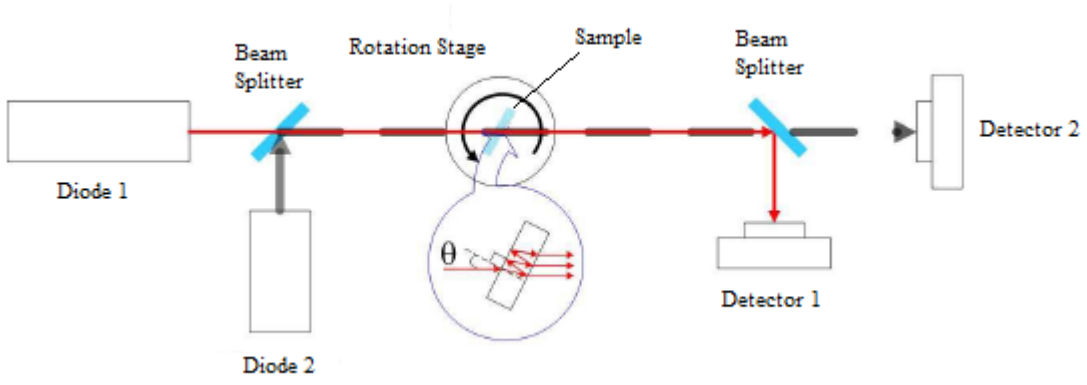

Figure 5: Two laser Fabry-Perot setup.[16]

It is important that the two beams are sent through collinear with each other. It is vital that the lasers be collinear through the sample in order to accurately solve for the two different refractive

indices. Because there are two different wavelengths two different fringes patterns are produced, with peaks occurring at different angles of incident of the sample. As before, you can solve for the peaks in fringes using equation 6 and setting ϕ_m equal to multiples of $2m\pi$ where m is an integer get

$$\phi_m = \sin^{-1}\sqrt{n^2 - \left(\frac{\lambda m}{2d}\right)^2}\,. \tag{9}$$

This equation is key to this method of measuring *n*, because when there is a peak in phase interference from each wavelength occurring at the same angle you can set equation 9 equal to itself for each of the wavelengths and accurately determine *d* and *n* for each wavelength. Now not every peak from each wavelength is going to overlap with the other one but there are definitely enough in each experiment to determine an accurate value for *d* and *n*.[16] Detailed discussion of the theory and data analysis of this method is beyond the scope of this investigation, for more information see Ref. 16.

There are a lot of benefits to using this method, the biggest being that there is not as much worry about outside influence because the Michelson interferometer is taken out of the process. As with the combined method you still get an extremely accurate measurement for *n* and *d* without having to know either prior to the experiment. Another advantage of this method is that it's faster than the combined method. You get a refractive index for two different wavelengths in only one data run instead of having to do two data runs to determine a refractive index for only one wavelength. The major problem with this setup is the same as in any Fabry-Perot interferometer, which is the need for the sample to have extremely flat and parallel sides.

IV. Assembly, Collimation and Characterization of the Laser Diodes

This section comprises the bulk of the work conducted during this project:

- Determining what diodes, controllers, electrical and optical components are needed
- Assembling the laser diodes
- Testing, optimizing and characterizing the propagation and focal properties of each laser diode

It is necessary for the light going through the sample to be collimated in order to ensure that the fringes you're measuring were indeed collinear in the material; meaning that the assumption that *d* is the same for both wavelengths is no longer valid. It also helps keep the signal strength of your measurements up. There are many conveniences of having the light be collimated; collimated light allows the system's set up to be more convenient, in that collimated light allows the path length to be much longer than that of a diverging light source. If you look at the schematics of the collimating tube in figure 6

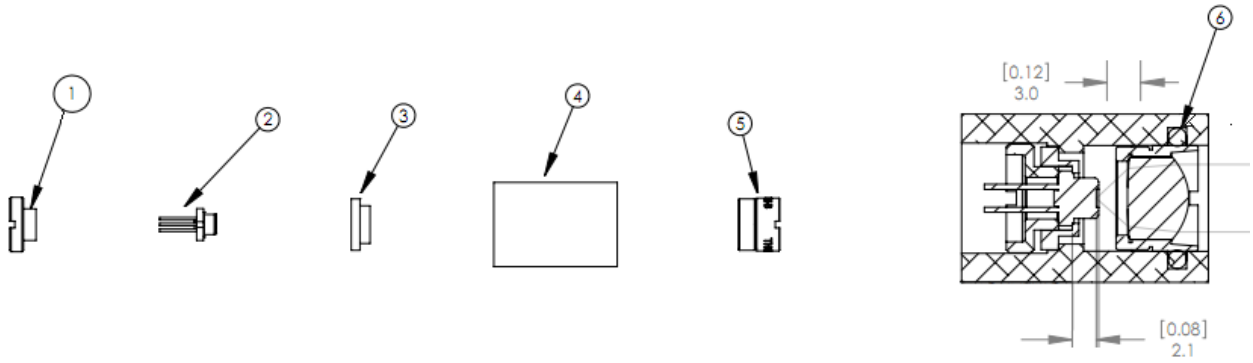

Figure 6: Schematics of laser collimating tube.[17]

you can see that there are six pieces to the collimating tubes of the diodes:

1. Retaining ring
2. Diode itself
3. Adapter
4. Collimating tube
5. Collimating lens
6. O-ring

The entire collimating setup can be taken in two parts, the diode side and the lens side. The collimating tube is just the holder for all the parts and diode. The first thing that goes in is the adapter to ensure that the diode isn't touching the lens after the lens is installed. Then the diode goes in followed by the retaining ring which locks the diode into place. The lens side is fairly easy to install but is highly time consuming to fine-tune. The only installation is screwing the lens mounted into the tube which is held in place by the friction provided by the O-ring. However, there is no set location for the collimating lens. This allows the collimating tube to be used for more than one wavelength. After everything is installed in the collimating tube the next step is to make sure the lens is in the proper spot for that particular diode. To do this you must measure the width of the laser at various distances from the collimating tube and make sure that the beam isn't converging or diverging. The more positions you measure the width at and the farther away you measure the beam the better collimated the laser will be. To change how well the beam is collimated the lens' position must be changed by screwing it farther in or out of the collimating tube. However, as most things, this isn't always as easy as it sounds. The biggest problem with collimating the diodes is the fact that most of the diodes do not have a perfectly circular profile. Due to the square design of the laser cavity, most of the diodes have an elliptical profile. This elliptical profile means that each axis does not have the same divergence angle and subsequently do not focus to the same point. Elliptical profiles also mean that it is impossible to collimate both axes at the same distance away from the collimating lens. The best way to

counteract this is to try and collimate the axis that focuses closer to the lens. That way there is a smaller divergence angle for the non-collimated axis.

There are eight Thorlabs laser diodes tested and measured in this project: two 639-nm, two 850-nm, two 980-nm and two 1310-nm. For each pair the lasers will be referred to as wavelength-A and wavelength-B (example 639-A and 639-B). The biggest problem with collimating the diodes is the possibility of each diode having an extremely different divergence angle. Table 1 shows the X and Y divergence angle of each diode.

Diode	X divergence angle (degrees)	Y divergence angle (degrees)
639-A	15.28	20.4
639-B	16.2	19.1
850-A	15.8	13.3
850-B	12.4	13.7
980-A	15.0	18.9
980-B	15.3	19.9
1310-A	21.7	21.0
1310-B	13.1	13.2

Table 1: Divergence angle of non-collimated diodes.

With the information from table 1 we know that there should only be a tiny amount of change needed when changing diodes in the collimating; it also helps having a collimating tube for each wavelength. It is good practice to check how well the diode is collimated before each data run, even if there has been no changing of the diodes.

It is helpful to know how the diodes behave before they have been collimated, but it is even more important to know how they behave after passing through the collimating tube. There are a few things to characterize about each diode after they have been collimated. Firstly, you must make sure that the beam is actually collimated by using the method described above. Of course it is unlikely to have the beam be perfectly collimated, especially for both axes, so the angle of divergence must be measured. It is also important to measure the Rayleigh range of each diode, which helps tell us how Gaussian the beam is. The first diode to be characterized is the 639-A diode, its beam profile can be seen in figure 7.

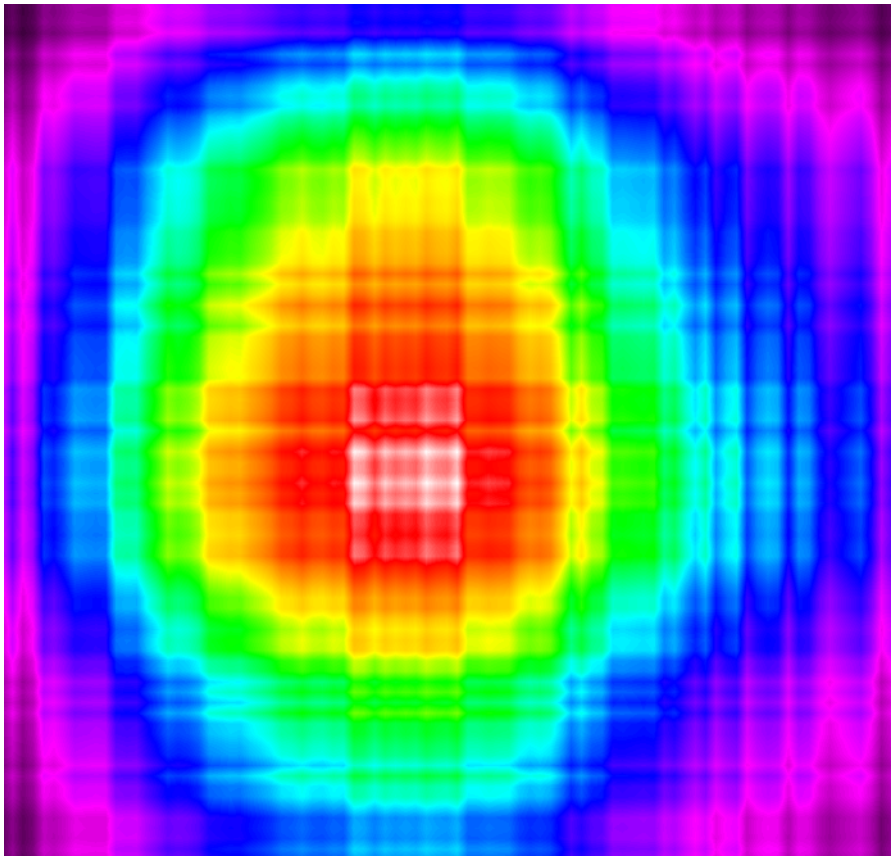

Figure 7: 639-A Beam Profile at z=100 cm from diode.

The image of figure 7 looks grainy because the diode's average power is fairly small, .91 mW after adjustment. This diode is fairly circular and collimated. The total divergence angle is .024 degrees and for the X and Y dimensions is .024 degrees and .025 degrees, respectively. The ellipticity and widths can be seen in table 2.

Distance from diode (cm)	X-width (μm)	Y-width (μm)	Ellipticity
110	3636	3444	.95
125	3728	3468	.93
140	3693	3421	.93
155	3718	3492	.94
170	3698	3479	.94
185	3771	3585	.95

Table 2: Ellipticity and Widths of 639-A.

Using a lens with a focal length of 150 mm the Rayleigh range, and minimum waist were measured and can be seen in table 3.

	X dimension	Y dimension	Total
Minimum waist (μm)	51.2	51.5	51.4
Measured Rayleigh range (mm)	1.77	1.22	1.50

Table 3: Rayleigh Range of 639-A.

The beam focusing to its minimum waist can be seen in figure 8.

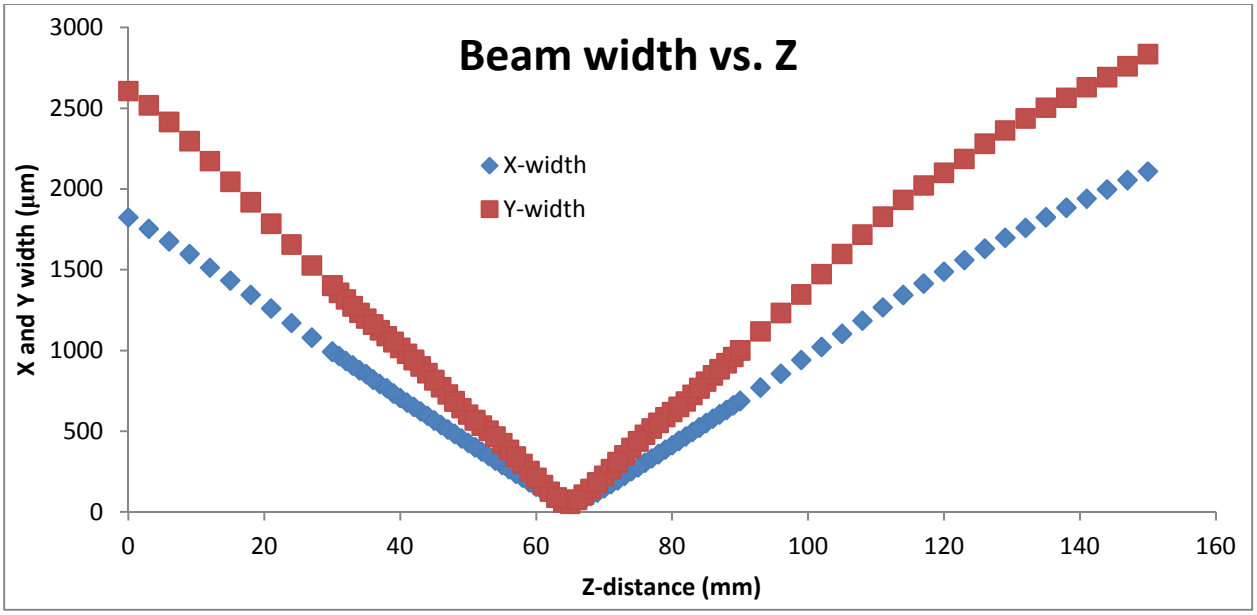

Figure 8: Focusing of 639-A.

The next diode analyzed is 639-B and its beam profile can be seen in figure 9.

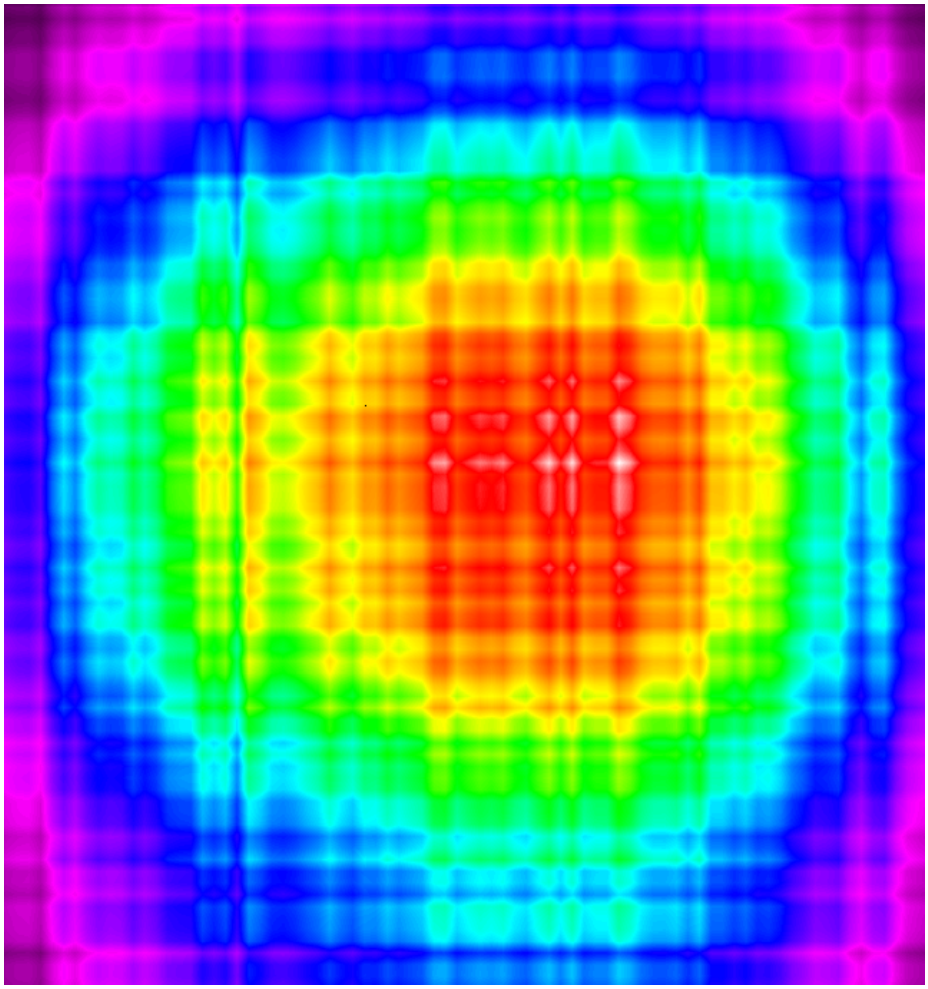

Figure 9: 639-B Beam Profile at z=125 cm.

Again this image looks grainy and for the same reason as 639-A (low power). The average power of this diode is .94 mW. This is not too surprising because the two diodes are the same model. This diode is a little better collimated and more circular than its counterpart. The total divergence angle is -.013 degrees and for the X and Y dimensions are -.021 degrees and -.005 degrees, respectively. The ellipticity and widths can be seen in table 4.

Distance from diode (cm)	X width (μm)	Y width (μm)	Ellipticity
110	3628	3522	.97
125	3611	3544	.98
140	3769	3670	.97
155	3613	3644	.99
170	3706	3745	.99
185	3717	3711	1

Table 4: Ellipticity and Widths of 639-B.

Using a lens with a focal length of 150mm the Rayleigh range, and minimum waist were measured and can be seen in table 5.

	X dimension	Y dimension	Total
Measured minimum Waist (μm)	56.6	58.9	57.7
Measured Rayleigh range (mm)	1.44	2.20	1.82

Table 5: Rayleigh Range of 639-B.

Figure 10 is shown to see how well the beam focuses down.

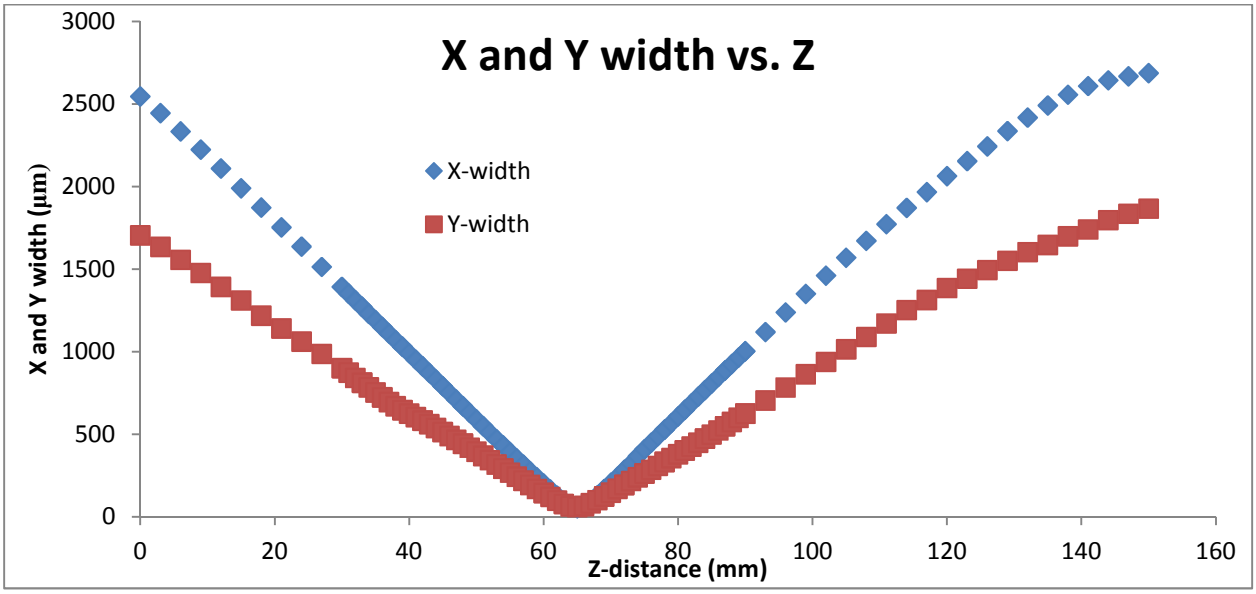

Figure 10: Focusing of 639-B.

The next diode on the list to be analyzed is the 850-A diode, its beam profile can be seen in figure 11.

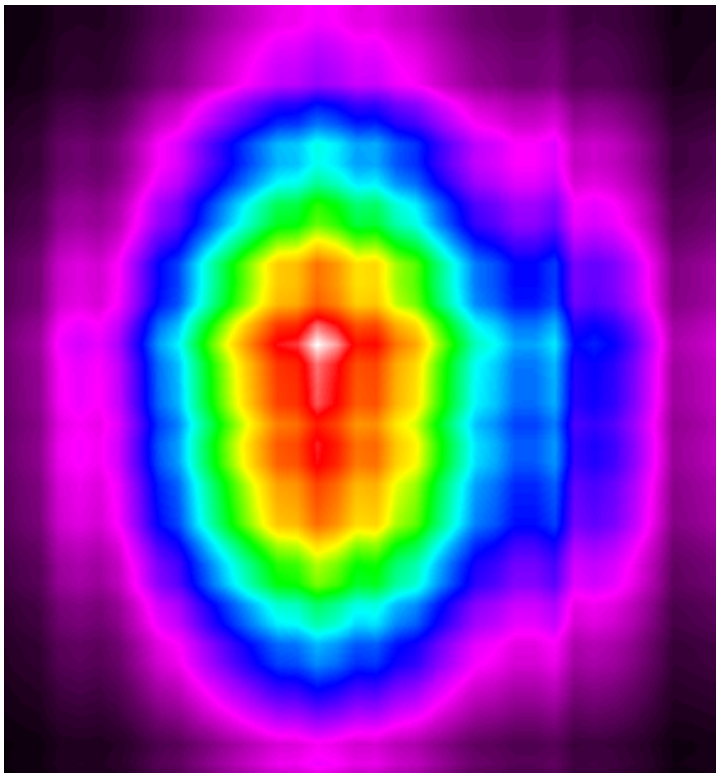

Figure 11: 850-A Beam Profile at z=125 cm.

This image looks much better than the previous two profiles and is in large part due to the fact that the average power is bigger, about 2.1 mW. As you can see in the profile, this diode is much more elliptical than the two 639-nm diodes. The total divergence angle is .037 degrees and for the X and Y dimensions is .048 degrees and .025 degrees, respectively. The ellipticity and widths can be seen in table 6.

Distance from diode (cm)	X width (μm)	Y width (μm)	Ellipticity
110	2307	1958	.85
125	2487	1945	.78
140	2808	2155	.77
155	3072	2267	.74
170	3459	2621	.76
185	3355	2717	.81

Table 6: Ellipticity and Widths of 850-A.

Using the same lens as before the Rayleigh range, and minimum waist were measured and can be seen in table 7.

	X dimension	Y dimension	Total
Measured waist (µm)	194.1	495.7	344.9
Measured Rayleigh range (mm)	2.86	9.74	6.30

Table 7: Rayleigh Range of 850-A.

Figure 12, below, shows how well the diode focuses down to its minimum waist.

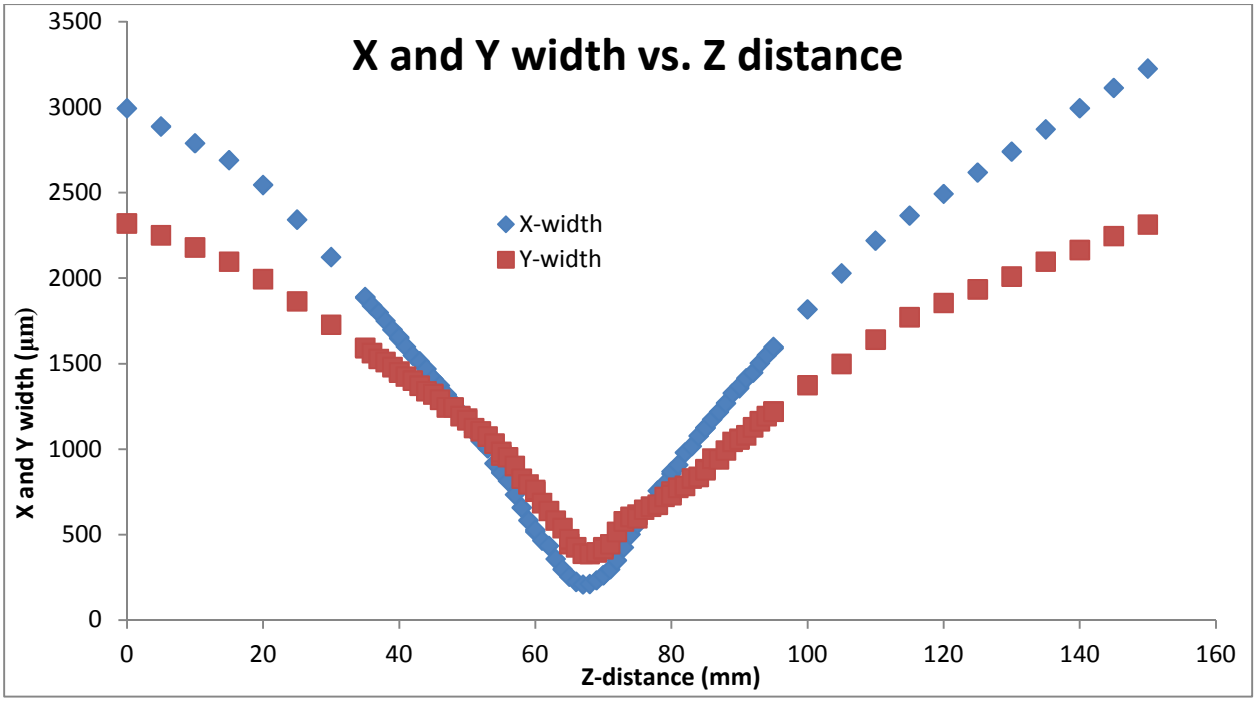

Figure 12: Focusing of 850-A.

The 850-B diode is the next one to be characterized; its beam profile can be seen below in figure 13.

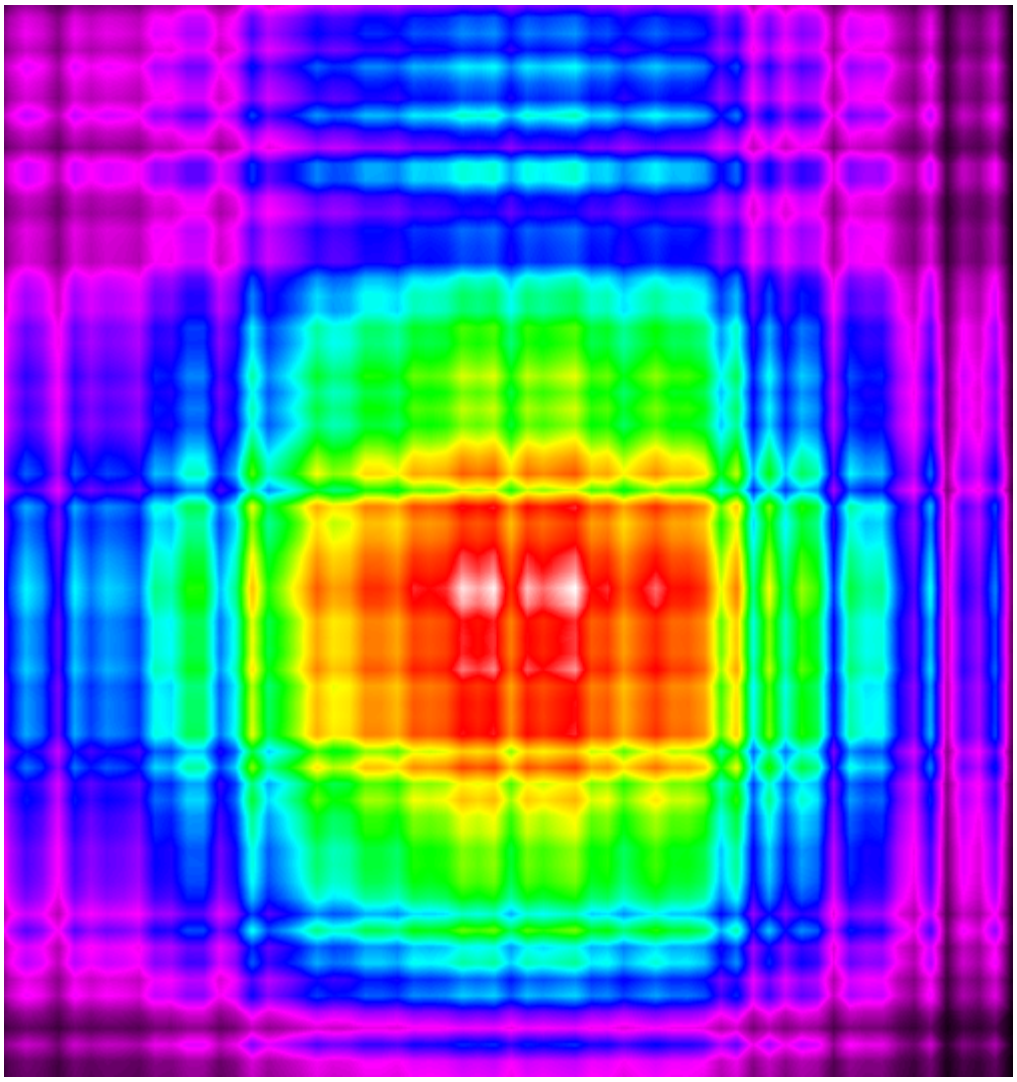

Figure 13: 850-B Beam Profile at z=170 cm.

This image resembles the two 639-nm diodes more in that it is grainier; again this is due to the diode having a smaller average power, about 1.13 mW. This diode is much more circular than its diode counterpart. The total divergence angle is .019 degrees and for the X and Y dimensions are .022 degrees and .015 degrees, respectively. The ellipticity and widths can be seen in table 8.

Distance from diode (cm)	X width (μm)	Y width (μm)	Ellipticity
110	3001	3089	.97
125	3113	3178	.98
140	3195	3245	.98
155	3246	3287	.99
170	3009	3094	.97
180	3031	3074	.99

Table 8: Ellipticity and Widths of 850-B.

The Rayleigh range, and minimum waist were measured using the same lens as before and the results are shown in table 9.

	X dimension	Y dimension	Total
Measured waist (µm)	103	1166	634
Measured Rayleigh range (mm)	1.2	19.6	10.4

Table 9: Rayleigh Range of 850-B.

Figure 14 shows how well the beam focuses. Here we can see a rather "non-Gaussian" focal behavior, and beam convergence and divergence.

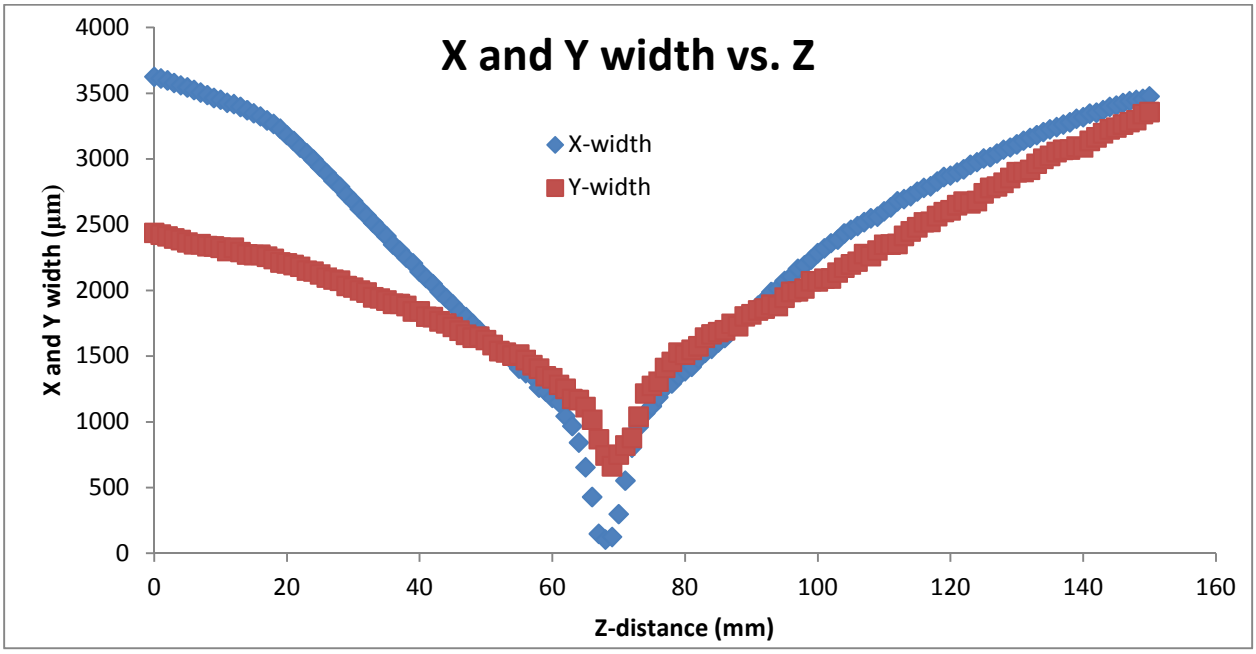

Figure 14: Focusing of 850-B.

The next diode to be analyzed is the 980-A diode; its profile can be seen in figure 15.

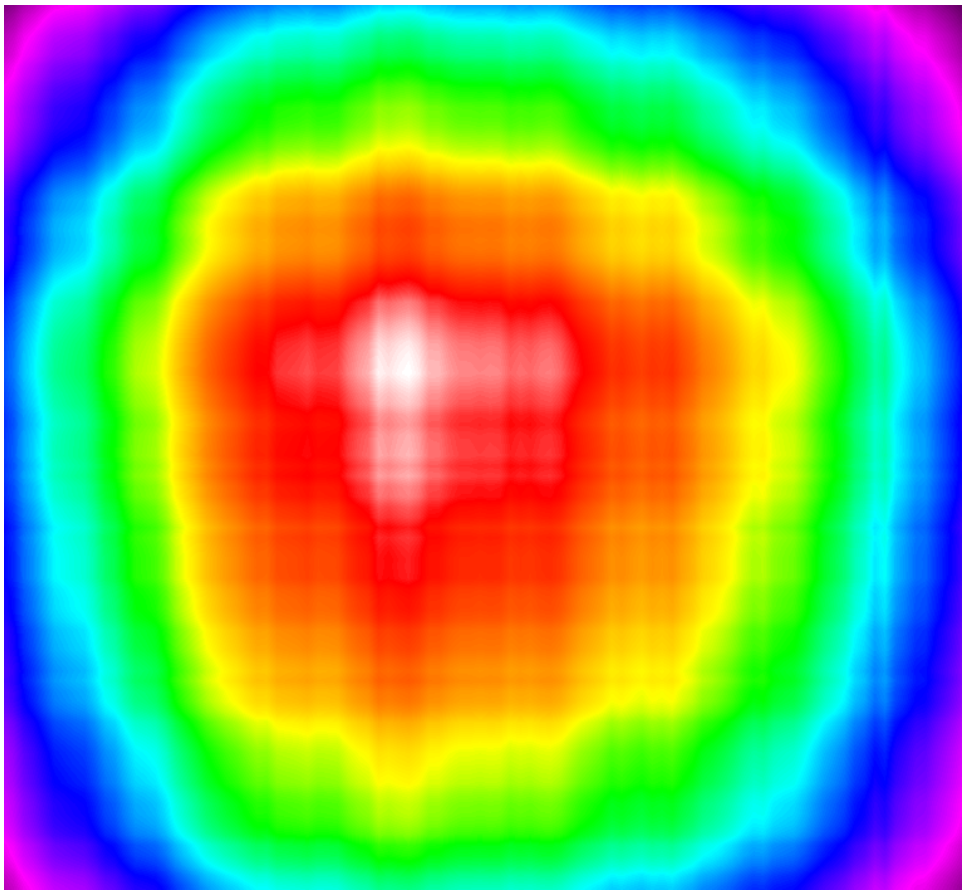

Figure 15: 980-A Beam Profile at z=140 cm.

This profile definitely looks better than all the previous ones because of its much higher average power, about 25 mW. This diode is also well collimated and circular. The total divergence angle is .012 degrees and for the X and Y dimensions are .013 degrees and .010 degrees, respectively. The ellipticity and widths can be seen in table 10.

Distance from diode (cm)	X width (μm)	Y width (μm)	Ellipticity
110	3969	3963	1
125	4013	3985	.99
140	4015	3968	.99
155	4042	3983	.99
170	4055	3966	.98
185	4078	4003	.98

Table 10: Ellipticity and Widths of 980-A.

The Rayleigh range and minimum waist were measured the same as the other diodes. The values can be seen in table 11.

.

	X dimension	Y dimension	Total
Measured waist (μm)	37.4	87.6	62.5
Measured Rayleigh range (mm)	.70	1.90	1.3

Table 11: Rayleigh Range of 980-A.

Figure 16 shows how well the beam focuses down to its minimum waist. The constant convergence and divergence angles between 10 cm and 130 cm from the diode illustrates the expected behavior of a Gaussian beam.

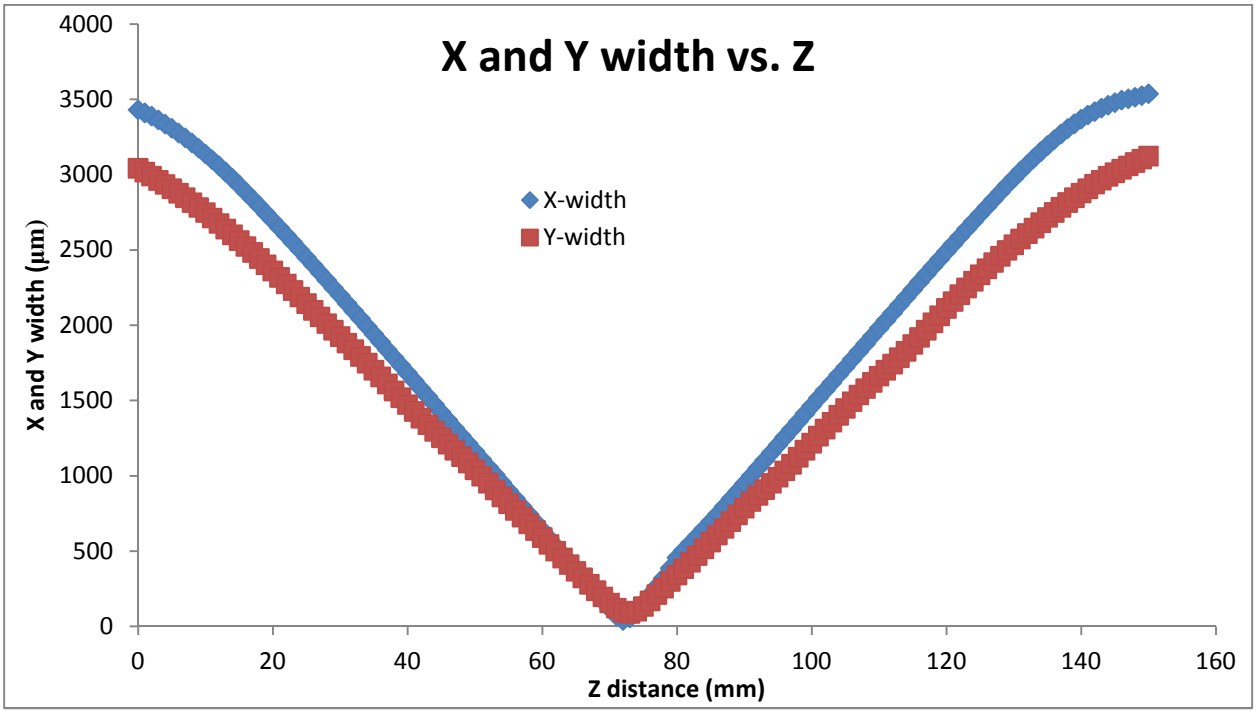

Figure 16: Focusing of 980-A.

The next diode on the list to be characterized is 980-B; its beam profile can be seen in figure 17.

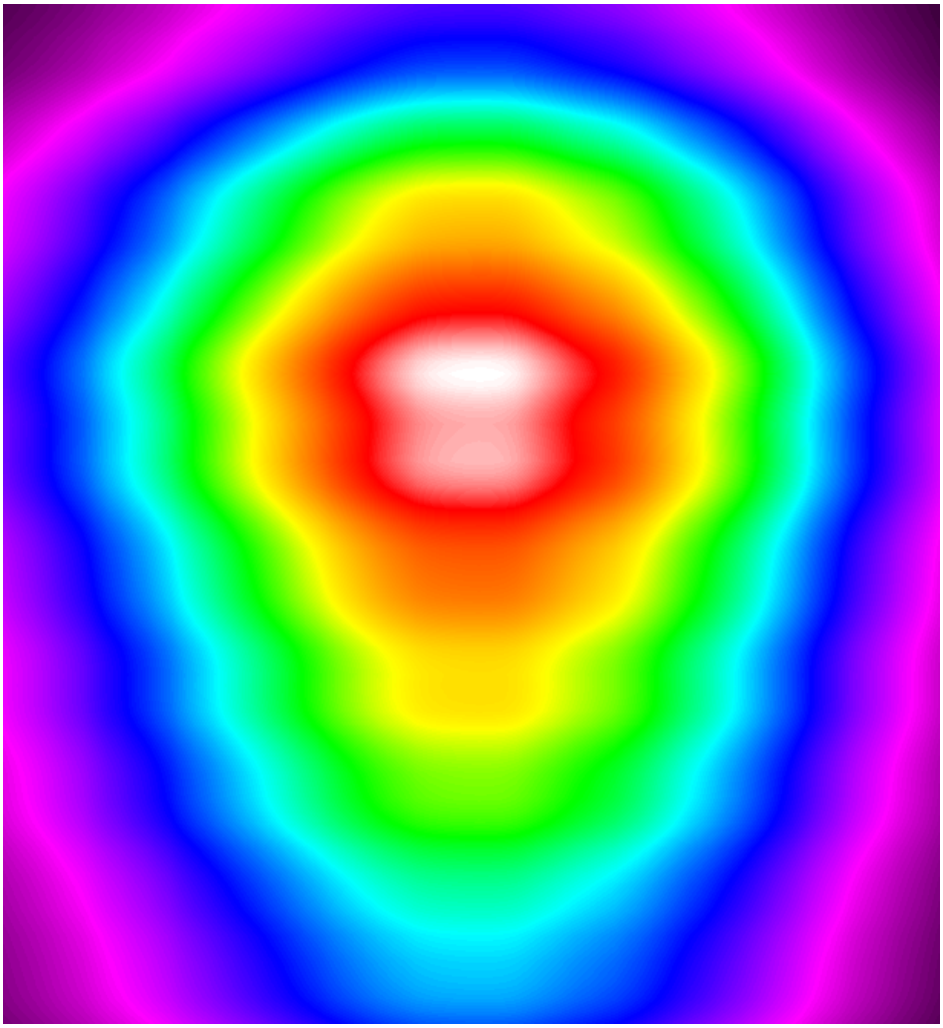

Figure 17: 980-B Beam Profile at z=110 cm.

This beam profile is similar to the other 980-nm diode in crispness but is not as circular as 980-A. The average power of this is diode is 62 mW. This diode is not as well collimated either. The total divergence angle is .011 degrees and for the X and Y dimensions are -.041 degrees and .065 degrees, respectively. The ellipticity and widths can be seen in table 12.

Distance from diode (cm)	X width (μm)	Y width (μm)	Ellipticity
110	3608	3095	.86
125	3591	3193	.89
140	3700	3525	.95
155	3642	3571	.98
170	3676	3573	.97
185	3636	3596	.99

Table 12: Ellipticity and Widths of 980-B.

The Rayleigh range and minimum waist were measured the same as the other diodes. The values can be seen in table 13.

	X dimension	Y dimension	Total
Measured waist (µm)	98.2	73.0	85.6
Measured Rayleigh range (mm)	2.78	1.63	2.21

Table 13: Rayleigh Range of 980-B.

Again, to see how well the beam focuses down to its minimum waist figure 18 is shown. This is another example of how a Gaussian beam converges and diverges.

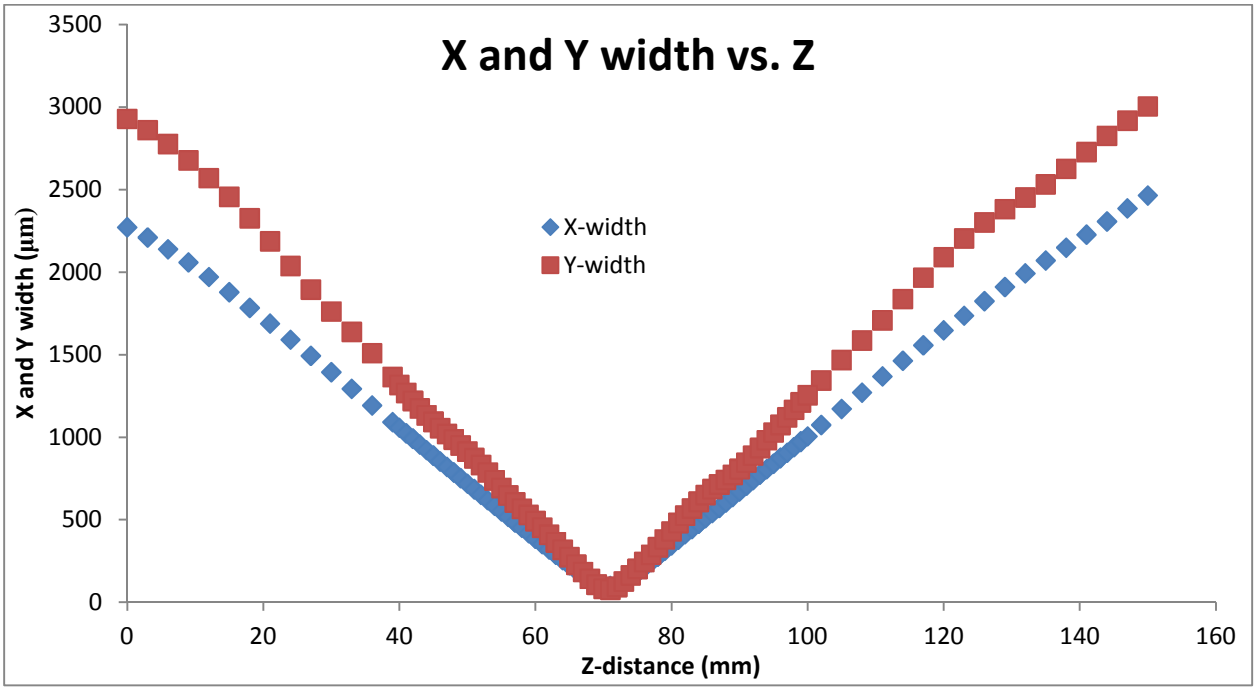

Figure 18: Focusing of 980-B.

The next diode to be characterized is the 1310-A diode; its beam profile is shown in figure 19.

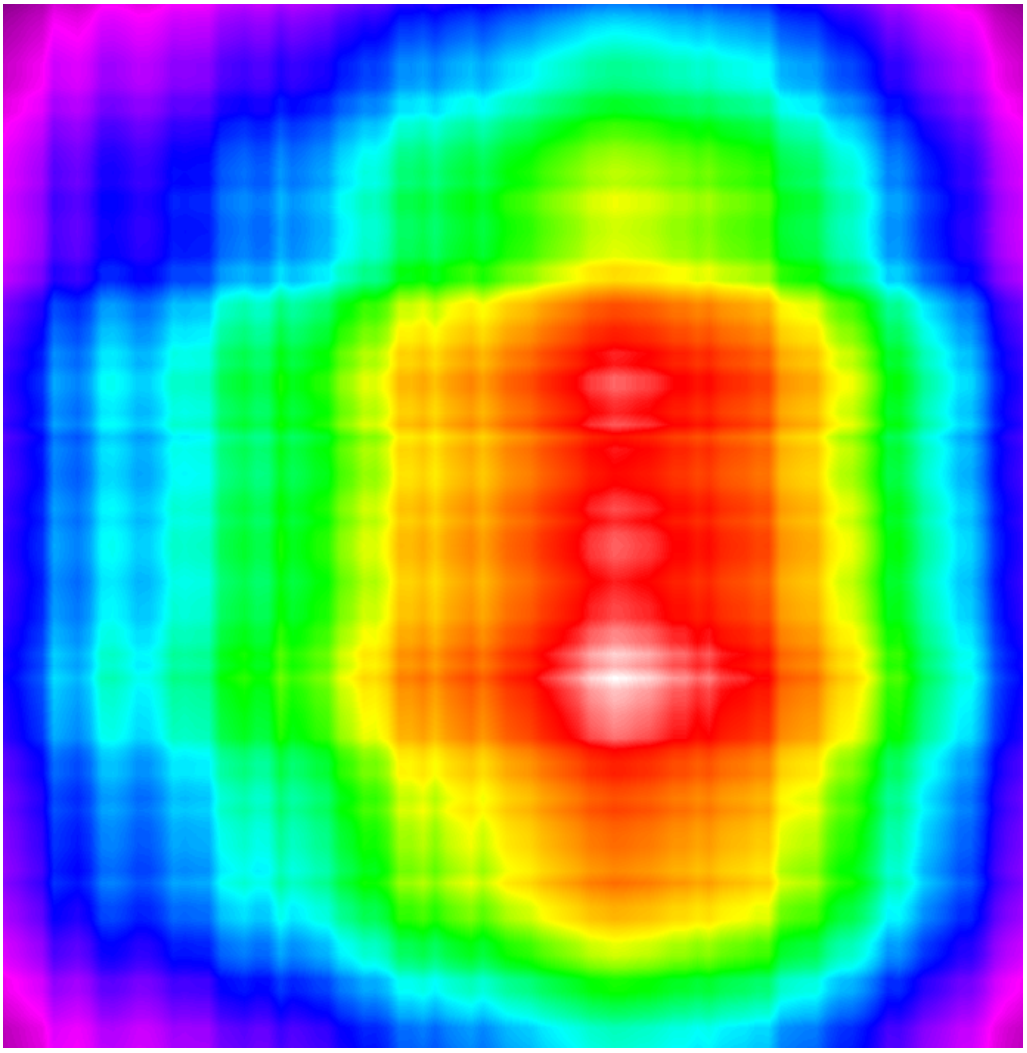

Figure 19: 1310-A Beam Profile at z=170 cm.

This beam profile is fairly elliptical and the ellipticity is constantly changing due to the differences in divergence angles in the two dimensions. The average power of this is diode is 22 mW. The total divergence angle is .019 degrees and for the X and Y dimensions are .001 degrees and .035 degrees, respectively. The ellipticity and widths can be seen in table 14.

Distance from diode (cm)	X width (μm)	Y width (μm)	Ellipticity
110	3877	3546	.92
125	3847	3568	.93
140	3922	3593	.92
155	3937	3618	.92
170	3871	3666	.95
185	3887	3710	.95

Table 14: Ellipticity and Widths of 1310-A.

The Rayleigh range and minimum waist were measured the same as the other diodes. The values can be seen in table 15.

	X dimension	Y dimension	Total
Measured waist (µm)	42.6	35.5	39.1
Measured Rayleigh range (mm)	.59	.47	.53

Table 15: Rayleigh Range of 1310-A.

Figure 20 shows how well the beam focuses down to its minimum waist. Unfortunately this is another example of a "non-Gaussian" beam behavior.

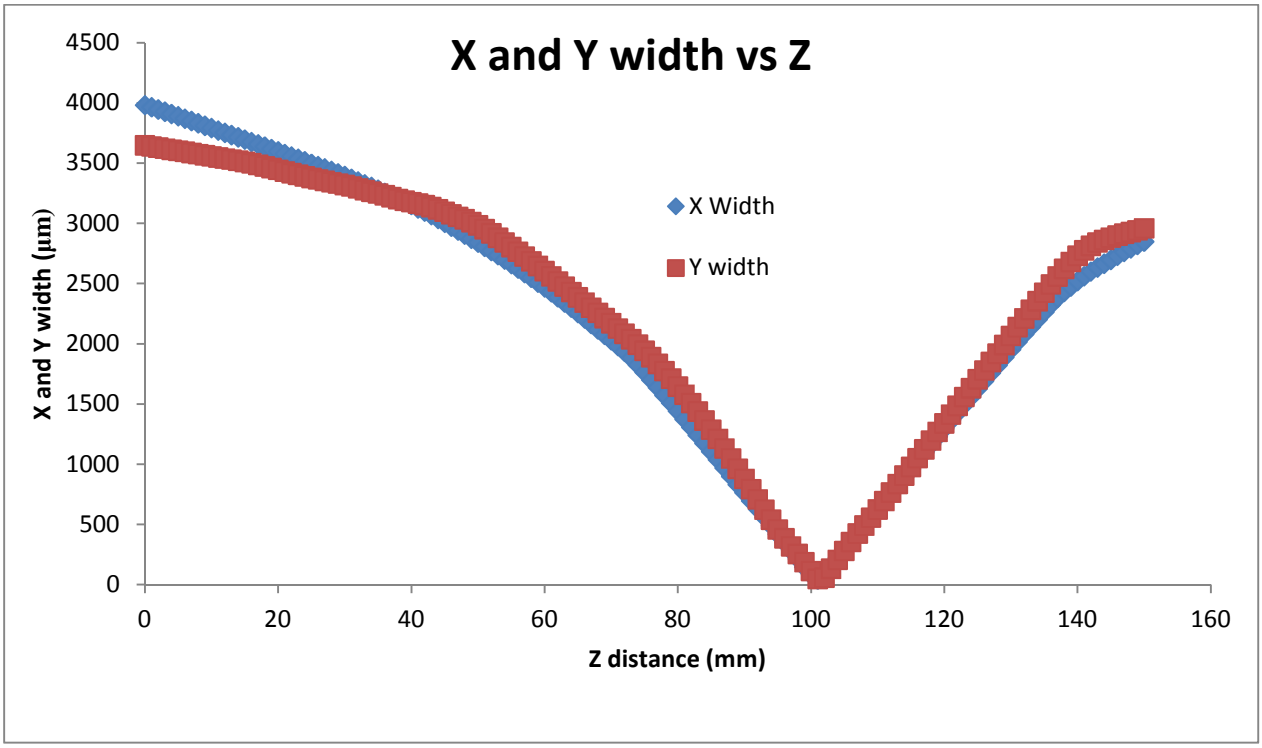

Figure 20:Focusing of 1310-A.

The final diode to be characterized is the 1310-B; its beam profile can be seen in figure 21.

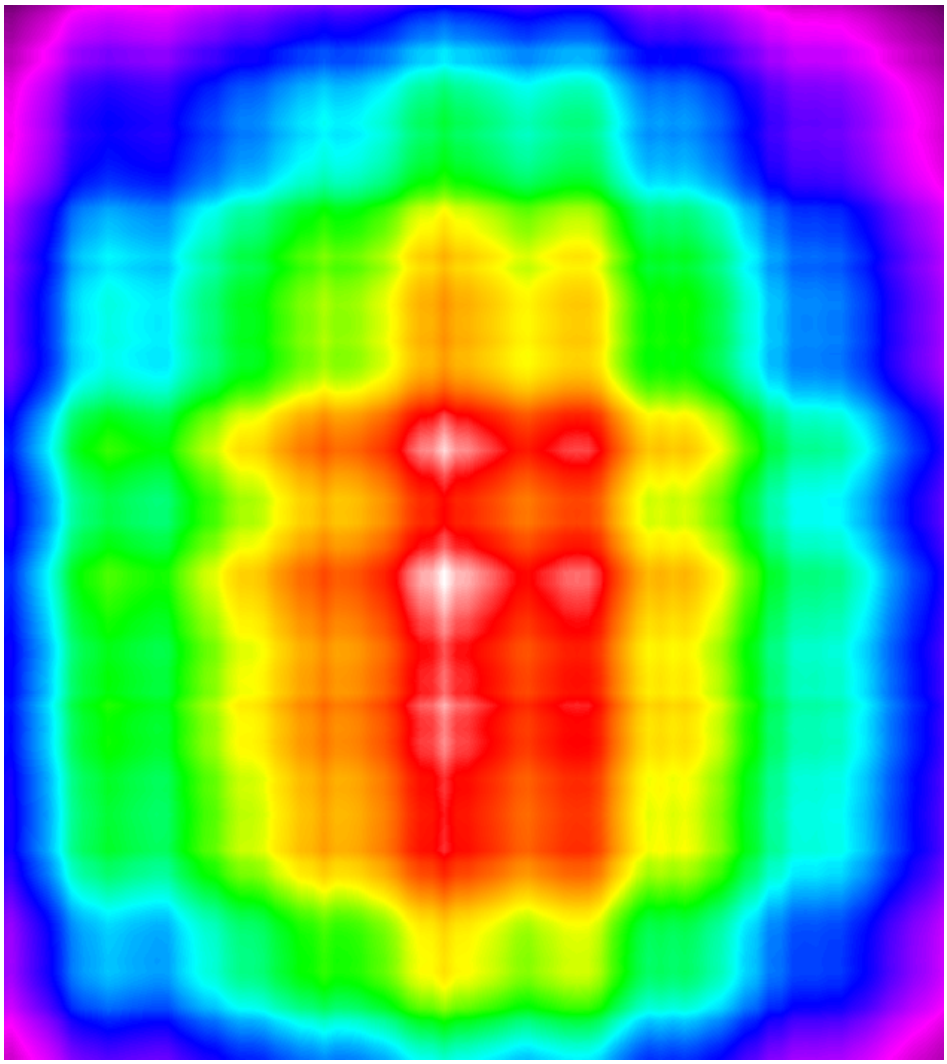

Figure 21: 1310-B Beam Profile at z=110 cm.

The average power of this diode is 33 mW. The profile shows a little ellipticity of the diode, but it does not change too much as the beam propagates. The total divergence angle of the beam is .032 degrees and the divergence angle for the X and Y dimensions is .085 and -.021 degrees, respectively. The ellipticity and widths can be seen in table 16.

Distance from diode (cm)	X width (μm)	Y width (μm)	Ellipticity
110	3510	3876	.91
125	3584	3859	.93
140	3578	3816	.94
155	3639	3806	.96
170	3664	3801	.96
185	3758	3776	.99

Table 16: Ellipticity and Widths of 1310-B.

The Rayleigh range and minimum waist were measured the same as the other diodes. The values can be seen in table 17.

	X dimension	Y dimension	Total
Measured waist (μm)	42.6	47.6	45.1
Measured Rayleigh range (mm)	.69	.64	.67
Theoretical Rayleigh range (mm)	4.36	5.44	4.88

Table 17: Rayleigh Range of 1310-B.

Figure 22 shows how well the beam focuses down to its minimum waist. Again this is an example of a beam that is not very Gaussian.

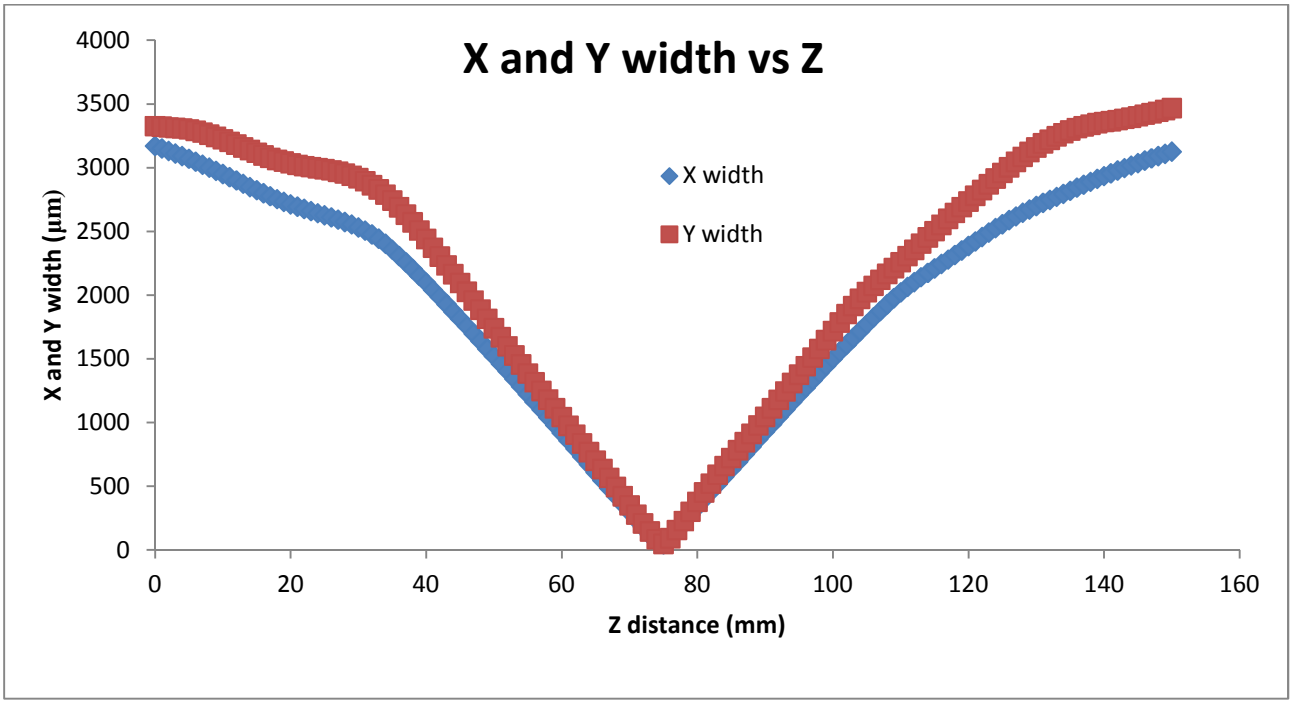

Figure 22: Focusing of 1310-B.

V. Preliminary Experimental Setup

The experimental setup of this version of the dual Fabry-Perot interferometer differs slightly from Choi setup. This setup can be seen in figures 23 through 26.

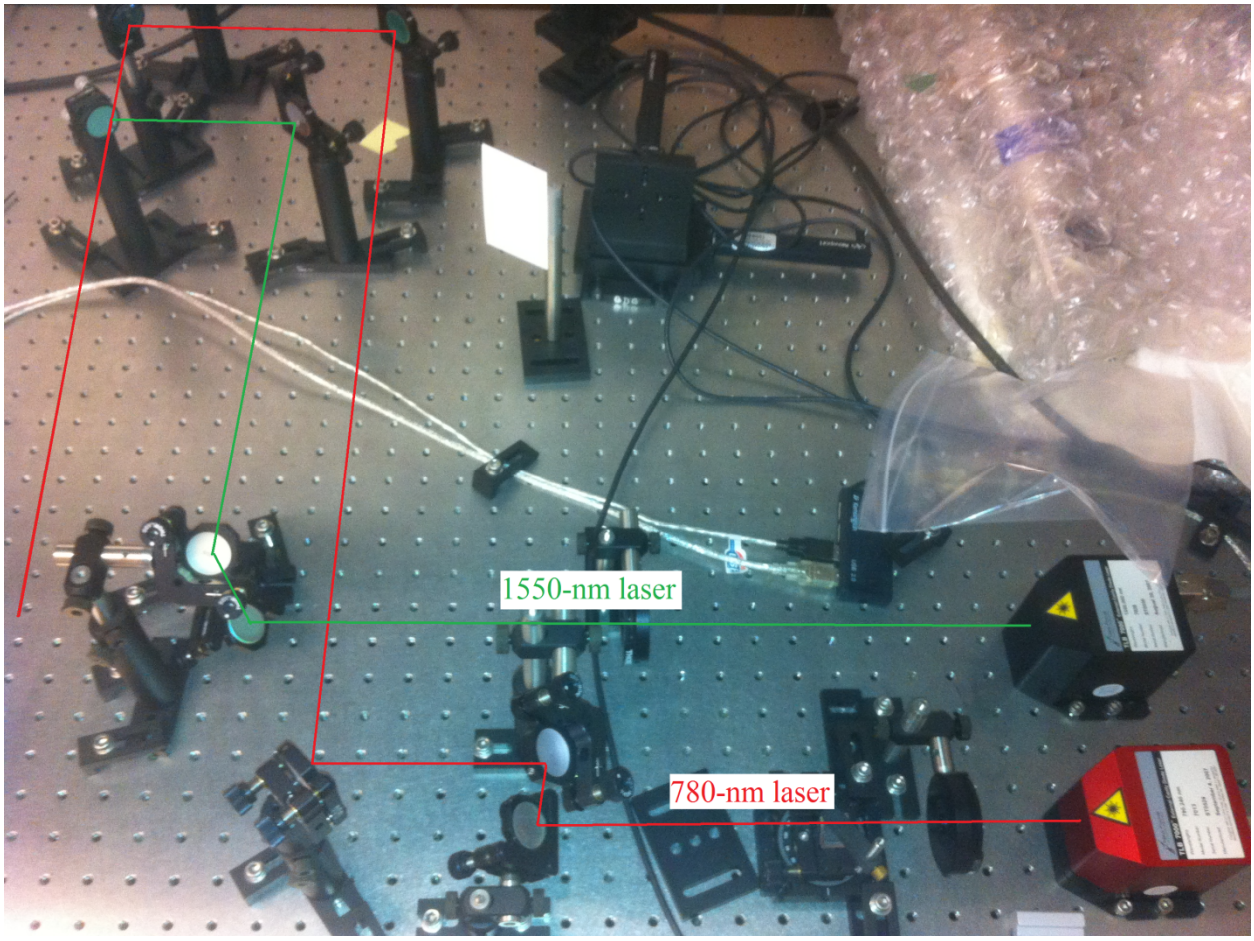

Figure 23: Setup for dual Fabry-Perot interferometer part 1.

In figure 23 the 780-nm and 1550-nm laser are shown separately, however once the beams start down the same path they will be represented as a red line.

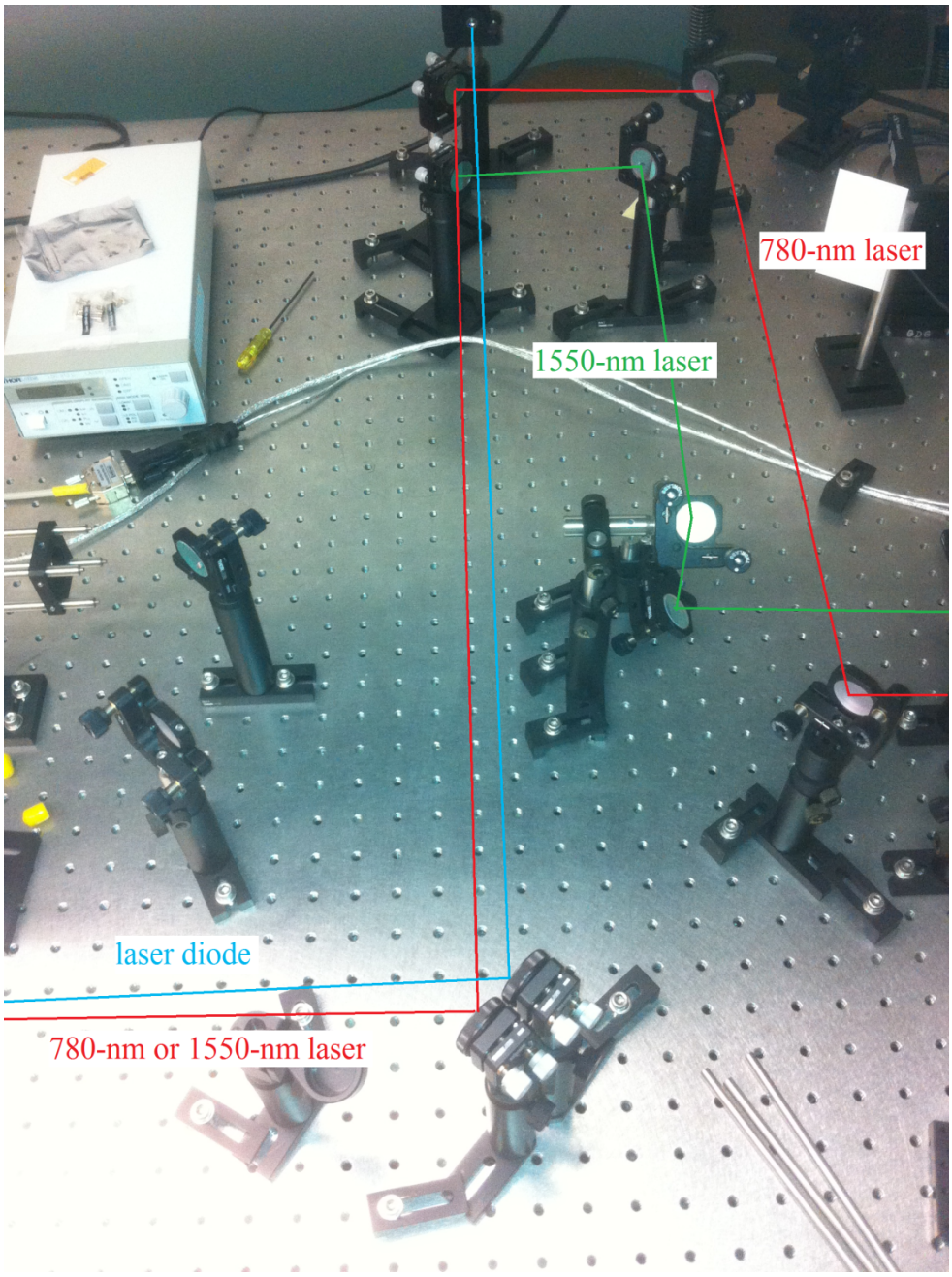

Figure 24: Setup of dual Fabry-Perot interferometer part 2.

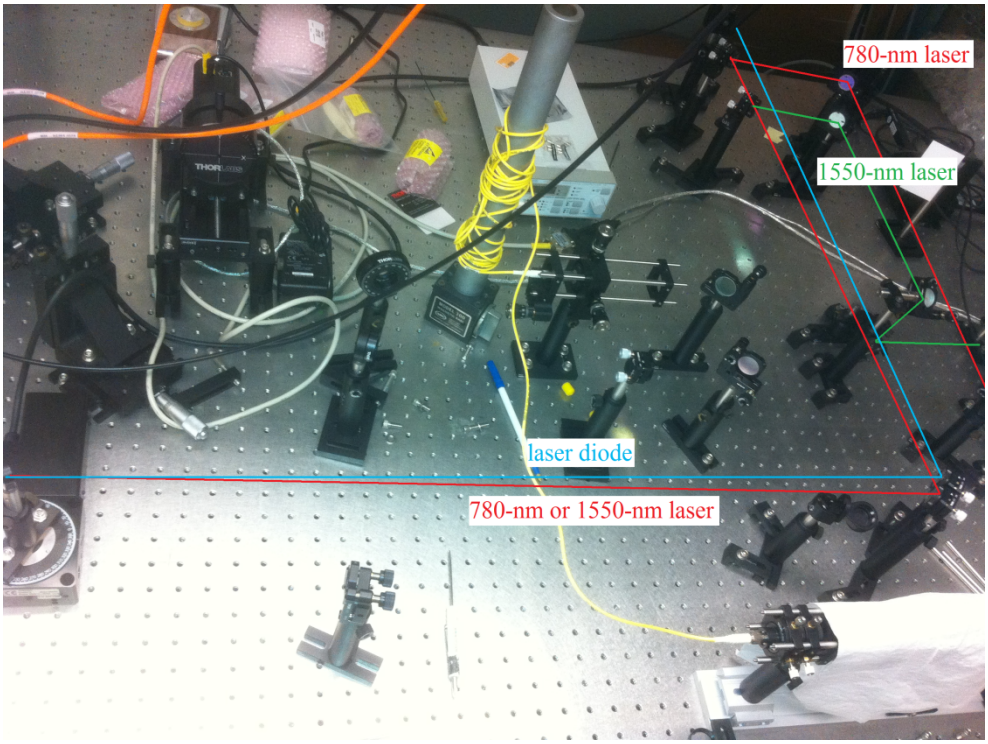

Figure 25: Setup of dual Fabry-Perot interferometer part 3.

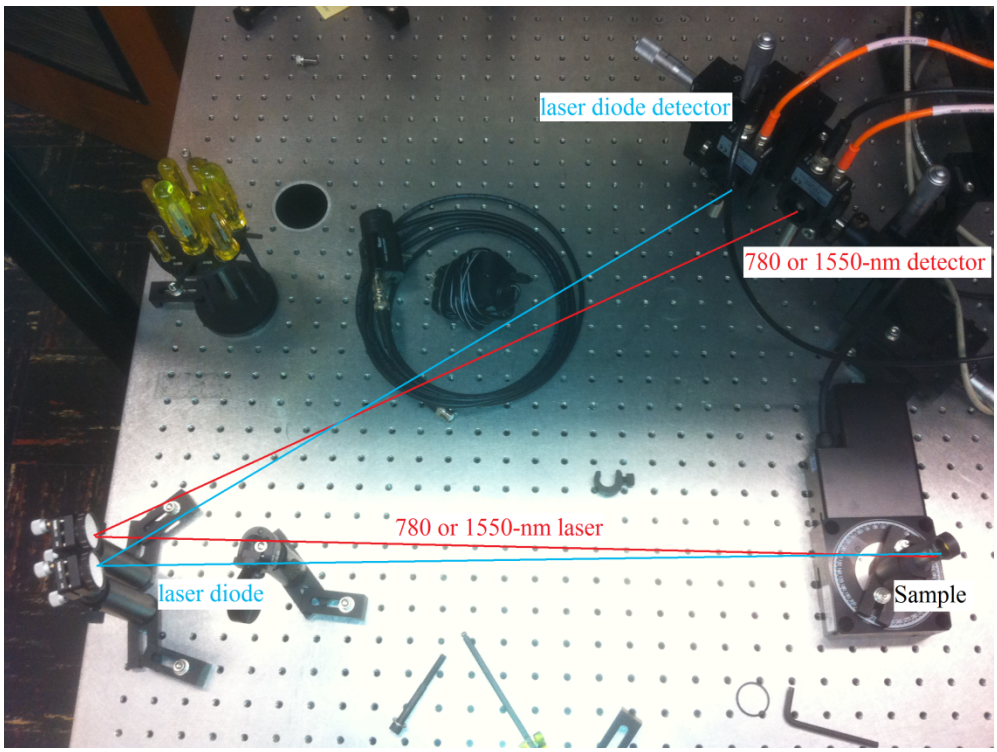

Figure 26: Setup of dual Fabry-Perot interferometer part 4.

This experiment required a lot of different pieces of equipment to run successfully, a complete list of all the equipment used can be seen in table 18.

Description	Vendor	Model Number
700-1800-nm detector	Thorlabs	PDA10CS
400-1100-nm detector	Thorlabs	PDA36A
Rotating step motor	Thorlabs	URS75PP
Lock-in Amplifier	Stanford Research Systems	SR830
Laser Diode Controller	Thorlabs	LDC210C
Optical Chopper	Thorlabs	MC1000A
Motion Controller	Newport	ESP300
Laser Controller	Vortex	6000
External-Cavity Diode Laser (780-nm)	New Focus	7013
External-Cavity Diode Laser (1550-nm)	New Focus	7028
Strain relief cable (x4)	Thorlabs	SR9A-DB9
Strain relief cable	Thorlabs	SR9D-DB9
Laser diode (639-nm) (x2)	Thorlabs	HL6358M6
Laser diode (850-nm) (x2)	Thorlabs	L850P030
Laser diode (980-nm) (x2)	Thorlabs	L980P030
Laser diode (1310-nm) (x2)	Thorlabs	ML725B8F
Collimating tube (x4)	Thorlabs	LT230P-B
Collimating tube	Thorlabs	LT230P-C-SP
Silver mirror (x6)	Thorlabs	PF10-03-P01-10
Beam Profiler (700-1800nm)	Thorlabs	BP104-IR
Beam Profiler Translation Stage	Micos	DC-B-026

Table 18: Complete list of equipment used.

VI. Results

The ultimate goal of this work was to show that the theory Choi proposed works. Without a working program to analyze the data it was not possible to determine the refractive index of any material. However, it was possible to observe the oscillatory behavior in intensities for both lasers as the sample was rotated. This observation of the oscillatory behavior is taken as a proof of principle for the dual Fabry-Perot interferometer system.

VII. Future Work

The next step of this overall project is to create a working Labview program which rotates the sample and record data from both detectors. This job is best done is stages, first developing a Labview VI which can rotate the sample at any given rate. The next step is to acquire the data from the detectors using an analog digital converter to speed up the process

compared to the lock in amplifier and collect the data using Labview. The following step would be to combine the Vis such that a single Labview program rotates the sample and collects data from the analog to digital converter. The final step would be creating a program or procedure, using any language (Matlab, Mathmatica, Igor, etc.), that takes the data which was collected and analyze it to determine the refractive indices for the two wavelengths and the sample thickness.

VIII. Conclusion

The goal of this project was a proof of theory to measure the refractive index of wafer shaped material using a two wavelength Fabry-Perot interferometer setup. To do this it was necessary to research and buy different laser diodes. The bulk of the work was spent assembling and characterizing the diodes. Once all the diodes were assembled and characterized it was shown that the theory of the two wavelength Fabry-Perot system was indeed correct, and the expected experimental intensity oscillations of each wavelength were observed.

Footnotes

1. Gilroy, EL. Hicks, MR. Smith, DJ. Rodger, A. "Viscosity of aqueous DNA solutions determined using dynamic light scattering." US National Library of Medicine 4159-63.
2. "Light through a prism." Why do objects have color. <http://apollo.lsc.vsc.edu/classes/met130/notes/chapter19/color.html>.
3. "Hot pavement." The Highway Mirage. <http://www.lyyn.com/news/newsletter/newsletter2007_03.html >.
4. Minimum Deviation by a Prism. February 27th, 2012. <http://www.mtholyoke.edu/~mpeterso/classes/phys103/geomopti/MinDev.html>.
5. Silicon. 1997. Process Specialties Inc. February 27th, 2012. <http://www.processspecialties.com/siliconp.htm>.
6. Bates, Seth. "Silicon Wafer Processing." Industry Initiatives for Science and Math Education (2000).
7. C. A. Proctor. "Index of refraction and dispersion with the intergerometer." Physics Review **24**, 185-201 (1907).
8. M.S. Shumate. "Interferometric measurement of large indices of refraction." Appl. Opt. **5**, 327-331 (1966).
9. G. D. Gillen, S. Guha. "Refractive-index measurements of zinc germanium diphosphide at 300 and 77 K by use of a modified Michelson interferometer." Appl. Opt. **10**, 2054-2058 (2004).
10. "The Michelson Interferometer." Interferometry. <http://www.scienceclarified.com/He-In/Interferometry.html#b>.

11. "Interference Fringes." Michelson Interferometer.
<http://en.wikipedia.org/wiki/File:Michelson_Interferometer_Laser_Interference_Fringes-Red.jpg>.
12. R. Nave. "Michelson Interferometer." HyperPhysics. February 27th, 2012.
<http://hyperphysics.phy-astr.gsu.edu/hbase/phyopt/michel.html>.
13. G. D. Gillen, S. Guha. "Use of Michelson and Fabry–Perot interferometry for independent determination of the refractive index and physical thickness of wafers." Appl. Opt. **3**, 344-347 (2005).
14. "Fabry-Perot Interferometer." Fabry-Perot Interferometer.
<http://www.starkeffects.com/Fabry-Perot-Interferometer.shtml>.
15. C. Fisher. "The Fabry-Perot Interferometer." The Wave Nature of Light. February 27th, 2012.
<http://www.phy.davidson.edu/stuhome/cabell_f/diffractionfinal/pages/fabry.htm#Theory>.
16. H. J. Choi, H. H. Lim, H. S. Moon, T. B. Eom, J. J. Ju, M. Cha. "Measurement of refractive index and thickness of transparent plate by dual-wavelength interference." Opt. Exp. **9**, 9429-9434 (2010).
17. Thorlabs. "Collimating tube schematics." Collimating Tubes.
<http://www.thorlabs.us/Thorcat/0800/0893-E0W.pdf>